Photophysics of Malonaldehyde: An ab Initio Study

Andrzej L. Sobolewski*,†,‡ and Wolfgang Domcke‡

Institute of Theoretical Chemistry, Heinrich-Heine-University, D-40225 Düsseldorf, Germany, and Institute of Physics, Polish Academy of Sciences, PL-02668 Warsaw, Poland

Received: January 4, 1999; In Final Form: March 29, 1999

Minimum-energy reaction paths and potential-energy profiles of the ground state and excited singlet states of malonaldehyde have been investigated using the ab initio CASSCF and CASPT2 methods. Hydrogen transfer (or proton transfer) as well as detachment of the hydrogen atom are considered as reaction coordinates. For the S_1 ($n\pi^*$) state, a proton-transfer barrier of about 3000 cm^{-1} is predicted, which is significantly larger than the barrier in the ground state (1100 cm^{-1}). The hydrogen bond in the S_1 ($n\pi^*$) state is found to be weaker than the H-bond in the ground state. For the S_2 ($\pi\pi^*$) state, on the other hand, an unusually strong H-bond and a barrierless potential-energy profile with respect to the proton-transfer coordinate are obtained. The single-minimum character of the S_2 ($\pi\pi^*$) potential-energy surface is definitively established via the calculation of the Hessian. The calculated normal modes and the vibrational spectrum of the S_2 ($\pi\pi^*$) state exhibit strong mixing of the OH stretch motion with CC and CO ring-stretching and ring-bending motions, reflecting pronounced bond conjugation within the H-chelate ring. Hitherto unknown $^1\pi\sigma^*$ and $^1n\sigma^*$ states have been identified which are strongly repulsive with respect to in-plane detachment of the mobile hydrogen atom, leading to low-lying conical intersections with the electronic ground state. Vibronic coupling of the $^1\pi\pi^*$ with the $^1\pi\sigma^*$ state by out-of-plane modes connects the former, via a low barrier, to the conical intersection of the latter state with the ground state, providing a mechanism for efficient internal conversion. It is argued that these findings reflect general properties of the H chelate ring in intramolecularly hydrogen-bonded molecules and can provide the explanation of the photostability of these systems.

1. Introduction

Malonaldehyde (MA) is the simplest molecule exhibiting a strong intramolecular hydrogen bond with a proton(hydrogen)-tunneling exchange between the oxygen atoms. It has been the subject of extensive experimental and theoretical studies over the years and has become the prototype model for a number of intramolecular proton-transfer (PT) systems. The transfer of a hydrogen atom from one heteroatom to another can be considered as one of the most fundamental reactions in chemistry, and plays a crucial role in many areas (for a review, see refs 1−4). The PT reaction involves a seemingly straightforward detachment/attachment mechanism, but since it involves the motion of a light atom, which is in turn strongly coupled to the remaining nuclear degrees of freedom, the process is characterized by a complex dynamical behavior that renders its theoretical characterization a challenging problem. The PT dynamics in malonaldehyde is a good example in this respect.[5]

As demonstrated conclusively by the pioneering studies of Wilson and collaborators,[6] the isolated molecule exists almost completely in one of the two equivalent planar asymmetric forms (C_s symmetry). Rapid hydrogen atom interconversion between these forms causes a tunneling splitting of the vibrational levels of the ground state, thus leading to a characteristic doubling of all rovibrational lines. The tunneling-induced splitting of the vibrationless (zero-point) level of the S_0 state was estimated from far-infrared spectroscopy to be about 21 cm^{-1}.[7] Later analysis of microwave data led to the value of 21.581 cm^{-1}.[8] A barrier height of about 6.6 kcal/mol (2300 cm^{-1}) for the PT reaction has been inferred from these experimental observations.[9] Ab initio quantum-chemical calculations based on the Hartree−Fock (HF) approximation have predicted a barrier of about 10 kcal/mol (3500 cm^{-1}).[12] The effect of dynamical electron-correlation on the PT barrier in the ground state of MA has been investigated with variety of theoretical methods. It has been concluded that dynamical electron correlation effects cause a significant reduction of the barrier, predicting a value in the range of 4−6 kcal/mol (1500−2000 cm^{-1}).[11−13] The calculated barrier is thus remarkably lower than the early estimates based on analysis of the experimental data in terms of a one-dimensional model (8 kcal/mol).[10] The analysis of Carrington and Miller based on a two-dimensional model[14] indicated that a barrier height of 6.6 kcal/mol is compatible with the experimentally observed value of the tunneling splitting. Similarly, the three-dimensional reaction-surface treatment of Shida et al.,[12] based on high-level ab initio calculations, gave a tunneling splitting in satisfactory agreement with the experimental data.

Apart from the analysis of the tunneling splitting of the vibrational ground level, no satisfactory agreement between observed and theoretically calculated vibrational IR spectra has been obtained so far despite extensive activity in the field.[6,15−17]

These facts reveal that the PT process in the electronic ground state involves a complex multidimensional dynamics even in this relatively simple system. The situation is much less transparent for the PT reaction in the excited electronic states of MA. In the near-UV region of the spectrum, Seliskar and Hoffmann[18] have identified a weak and highly structured absorption band, which has been assigned to the $S_0 \rightarrow {}^1n\pi^*$ electronic transition. The band origin, associated with a promi-

* Corresponding author. E-mail: sobola@ifpan.edu.pl.
‡ Institute of Theoretical Chemistry.
† Institute of Physics.

10.1021/jp990030s CCC: $18.00
Published on Web 05/25/1999

nent feature at 28273 cm^{-1}, exhibits a splitting of roughly 7 cm^{-1}, which has been attributed to the change of the tunneling splitting with respect to the ground state. The progression forming modes with frequencies of 185 and 1300 cm^{-1} were assigned to in-plane H-chelate-ring-bending and carbonyl stretching modes. Each of these progressions shows a characteristic doubling of the vibrational structure. The $0^+/0^-$ term level splitting of the S_1 ($n\pi^*$) state has been calculated to be about 14 cm^{-1} on the basis of the ground-state value of 21 cm^{-1}.[18] Both the reduced splitting and the long Franck−Condon envelope of the vibrational progressions suggest that the potential-energy (PE) surface of the S_1 ($n\pi^*$) state is significantly distorted relative to the ground state and has a more open, i.e., less tightly bonded, O−H···O structure. This implies that the barrier for the PT reaction increases upon $n \rightarrow \pi^*$ electronic excitation. It has also been conjectured by Seliskar and Hoffmann that vibrational out-of-plane modes of a_2 symmetry are involved in Herzberg−Teller intensity borrowing from the nearby $S_0 \rightarrow S_2$ ($\pi\pi^*$) transition.

Ab initio calculations of the barrier in the lowest excited singlet states of MA have been performed by Luth and Scheiner.[19] Using the CI singles method (CIS), these authors predicted a significant increase of the barrier in the S_1 ($n\pi^*$) state and its reduction in the S_2 ($\pi\pi^*$) state as compared to that in the ground state. However, both excited-state barriers have been found to disappear when electron correlation effects are included via second-order Møller−Plesset perturbation theory. It was thus concluded that the PE surfaces of these states are barrierless with respect to the PT reaction.[19]

In a recent high-resolution degenerate four-wave mixing spectroscopic study of the origin region of the $S_0 \rightarrow S_1$ ($n\pi^*$) transition in MA, Arias et al.[20] have determined a splitting of 19 cm^{-1}, which differs significantly from the 7 cm^{-1} value of Seliskar and Hoffmann.[18] Assuming a 21.6 cm^{-1} splitting in the ground state, this leads to an estimate of the splitting in the S_1 ($n\pi^*$) state of barely 2.5 cm^{-1}, thus suggesting a substantial increase of the PT barrier in this state. In view of the discrepancy of these estimates with the ab initio predictions of Luth and Scheiner, Arias et al. have reinterpreted their data, assuming an increase of the tunneling splitting to about 40 cm^{-1} in the S_1 ($n\pi^*$) state, implying a significant decrease of the PT barrier in the S_1 state relative to the S_0 state.

It is clear from the above overview that the spectroscopy and dynamics of MA are far from being precisely understood. This has motivated us to perform a comprehensive ab initio investigation of the excited states of MA. We employ the complete-active-space self-consistent-field (CASSCF)[21] method for geometry optimizations and for the calculation of harmonic frequencies, while electron correlation effects beyond this approximation were included employing second-order perturbation theory with respect to the CASSCF reference (CASPT2).[22] An essential feature of the calculations is the choice of a judiciously selected active space which includes the most relevant σ an σ^* orbitals and thus accounts for the most significant $\pi\sigma$ and $\sigma\sigma$ correlation effects. Excited-state minimum-energy paths and the corresponding PE profiles for the motion of the hydrogen atom are constructed. We confirm previous conjectures[19] on the barrierless nature of the $^1\pi\pi^*$ state. For the S_1 ($n\pi^*$) surface, on the other hand, a significant barrier with respect to the PT reaction is predicted. Novel aspects of these calculations are the determination of the vibrational normal modes at the symmetrical minimum of the $^1\pi\pi^*$ surface and the identification of low-lying $^1\pi\sigma^*$ and $^1n\sigma^*$ excited singlet states which intersect the $^1n\pi^*$ and $^1\pi\pi^*$ states and are thus of relevance for the rationalization of the photochemical dynamics. We identify, moreover, a low barrier on the PE surface of the S_1 state with respect to hydrogen detachment as well as a low-lying conical intersection of the S_1 and S_0 PE surfaces, which can account for efficient internal conversion to the ground state. Preliminary results of present investigations have been reported in ref 23.

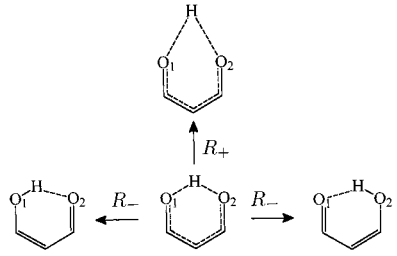

Figure 1. Hydrogen-transfer (R_-) and hydrogen-detachment (R_+) reaction coordinates of malonaldehyde considered in this work.

2. Computational Details

The system and the reaction coordinates examined in the present work are illustrated in Figure 1. The hydrogen-transfer coordinate is defined as the difference of the two OH distances, $R_- = (R_{O_1H} - R_{O_2H})/2$, and the hydrogen-detachment coordinate is defined as $R_+ = (R_{O_1H} + R_{O_2H})/2$. Previous studies of the reaction have led to the conclusion that this process is more properly called hydrogen-transfer (HT) rather than proton-transfer (PT) reaction, but the literature in the field has accepted the latter phrase for this process.[1−4] Thus, in the following we use the acronym PT for the hydrogen-transfer reaction and PD for the hydrogen-detachment reaction.

In the study of the reaction paths the coordinate-driven minimum-energy-path approach has been adopted, i.e., for a given value of R_{O_1H} (or R_{O_2H}) all remaining intramolecular coordinates (including R_{O_2H} or R_{O_1H}, respectively) have been optimized in each electronic state. For the PT reaction path, C_s symmetry (i.e., planarity of the molecular frame) was imposed, while C_{2v} symmetry was enforced for the PD reaction path, if not otherwise specified. Note that in C_{2v} symmetry $R_+ = R_{O_1H} = R_{O_2H}$. The reaction-path calculations have been performed at the CASSCF level with the GAMESS program package.[24] At the stationary points of the PE surfaces, a normal-mode analysis has been performed, employing the analytically calculated Hessian as implemented in GAUSSIAN94.[25] The 6-31G** valence double-ζ basis set with polarization functions on all atoms[26] has been used for geometry optimizations and for calculations of the Hessian.

The canonical Hartree−Fock orbitals of MA which are considered as active orbitals in the CASSCF calculations are displayed on the left-hand side of Figure 2. They include the full set of π orbitals (1-3b_1 and 1-2a_2 in the C_{2v} point group), the highest n lone-pair orbital (7b_2), and a pair of σ and σ^* orbitals (9a_1 and 10a_1, respectively) mostly localized on the O−H−O molecular moiety. The σ orbitals which appear to be crucial for qualitatively correct description of the PE profile for the PT reaction in the $^1\pi\pi^*$ state in the CASSCF approximation include the lone-pair orbital and the σ^* orbital, which has nodes on the OH bonds (see Figures 2 and 3). The totally symmetric partner of the σ^* orbital was included for completeness into the active space, but this does not lead to qualitative changes of the results. It should be mentioned in this context that these orbitals in their Hartree−Fock form almost do not contribute to the lowering of the CASSCF energy. The electron-correlation effects included in the CASSCF treatment

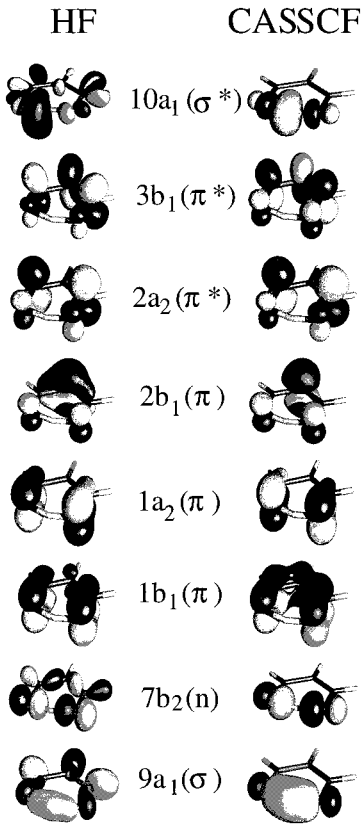

Figure 2. Hartree-Fock (HF) and CASSCF orbitals of MA determined at the C_{2v} stationary point of the $^1\pi\pi^*$ state.

force them, however, to relax and to localize almost exclusively on the O−H−O molecular moiety (Figure 2). The localization is a consequence of the incompleteness of the σ orbital active space (see ref 27 and references therein). This effect is not observed for the π orbitals, since the complete set of them was included into the active space. Further extension of the σ active space does not noticeably change the results but significantly increases the cost of the calculations. These studies at the CASSCF level uniqely identify the σ orbitals which are most important for the theoretical description of the PT reaction in MA.

To illustrate the relevance of a proper selection of the active space used in the CASSCF calculations, we present in Figure 3 results obtained for the $^1B_2$ ($\pi\pi^*$) state of MA optimized with C_{2v} symmetry constraint. Three quantities, the CASSCF energy, the vibrational harmonic frequency of the PT mode (involving mostly the R_- coordinate), and the frequency of the PD mode (involving the R_+ coordinate), are plotted vs the size of the active space. The minimal active space used for the description of the $^1B_2$ ($\pi\pi^*$) state of MA (CAS no. 1 in Figure 3) includes the five π-orbitals (1-3b_1 and 1-2a_2). The C_{2v} geometry of MA in the $^1B_2$ ($\pi\pi^*$) state optimized with this active space represents a transition state with respect to the PT reaction (ω_{PT} = i 941 cm^{-1}) and exhibits a vibrational frequency ω_{PD} = 1994 cm^{-1} with respect to PD reaction. Note that the value of ω_{PD} is very low in comparison with typical OH stretch frequencies. Inclusion of the highest lone-pair orbital (7b_2) into the active space (CAS no. 2) does not substantially change these quantities. Similarly, replacing the 7b_2 orbital by the σ^* orbital (10a_1), which is mostly localized on the O−H−O molecular moiety and has nodes along the OH bonds, this has only very little influence on the results. The situation changes qualitatively when both n and σ^* orbitals are included into the active space (CAS no. 4). Now ω_{PT} is real, indicating that the C_{2v}-optimized

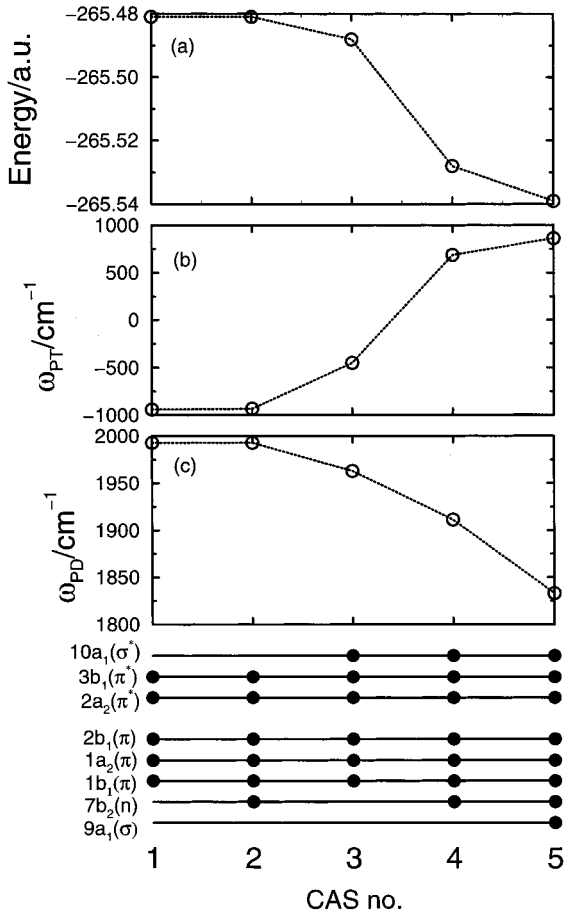

Figure 3. (a) The CASSCF/6-31G** energy, (b) the vibrational frequency involving hydrogen motion along the PT coordinate, and (c) along the PD coordinate, calculated at the C_{2v} stationary point of the $^1\pi\pi^*$ state of MA vs the size of the active space. Dots in the lower part of the figure denote orbitals included in the active space. The S_2 (C_{2v}) structure is a first-order saddle point, see Table 2.

geometry with the hydrogen atom midway the oxygens represents the minimum of the PE profile in the $^1B_2$ ($\pi\pi^*$) of MA with respect to the PT reaction. A further extension of the active space by including an additional σ orbital (9a_1), the bonding counterpart of 10a_1 (σ^*), does not noticeably change ω_{PT}, but leads to a further decrease of ω_{PD} (note, however, the difference in the scale between Figure 3b and c). CAS no. 5 was the most extended active space which could be employed for efficient analytical evaluation of the Hessian.

Although MA is a relatively small polyatomic molecule, it is not possible to perform full-valence CASSCF calculations. Therefore the remaining electron-correlation effects not recovered at the CASSCF level are partly of dynamical and nondynamical character, as far as the σ and σ^* orbitals are concerned. The remaining electron-correlation effects on the PE profiles have been treated at the level of second-order perturbation theory with the CASSCF wave function as the reference (CASPT2) using the MOLCAS-4 program package.[28] For these single-point calculations the ANO-L(3s2p1d/2s1p) basis of valence double-ζ (plus polarization) quality implemented in MOLCAS-4 has been used.

Three active spaces have been used in the CASSCF/CASPT2 calculations: (i) a "small" active space which includes the π orbital only (CAS no. 1 of Figure 3), (ii) a "medium" active space (CAS no. 5 of Figure 3), and (iii) an "extended" active space (CAS no. 6) which includes four additional σ type orbitals (as compared to the medium active space), two of which are

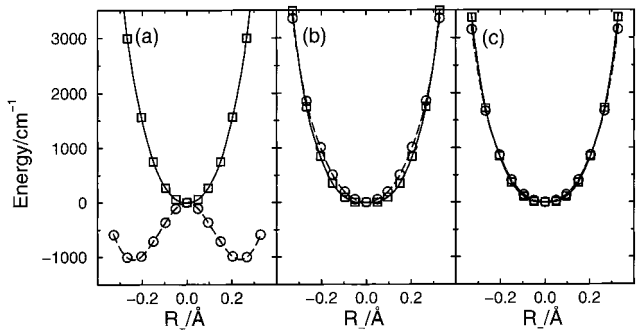

Figure 4. (circles) CASSCF and (squares) CASPT2 PE functions of the $^1B_2$ ($\pi\pi^*$) state of MA, calculated with the (a) small, (b) medium, and (c) extended active space as a function of the R_- reaction coordinate. The energy at $R_- = 0$ is defined as the zero of the energy scale.

TABLE 1: Symmetry Labels of Molecular Orbitals Used in CASSCF Calculations for Various Symmetry Groups

CASSCF: N_{el}/N_{orb}	"small" 6/5	"medium" 10/8	"extended" 14/12
C_{2v}	[1-3b$_1$, 1-2a$_2$]	[9-10a$_1$, 1-3b$_1$, 1-2a$_2$, 7b$_2$]	[8-11a$_1$, 1-3b$_1$, 1-2a$_2$, 6-8b$_2$]
C_2	[1-2a, 1-3b]	[9-12a, 7-10b]	[8-13a, 6-11b]
C_s	[1-5a″]	[15-17a′, 1-5a″]	[13-19a′, 1-5a″]

occupied and two are virtual in the HF reference. The enumeration of orbitals for the three active spaces defined above in the different symmetry point groups is given in Table 1. For the description of the $n\pi^*$ electronic state the small active space includes the n orbital in addition to the π orbital space, so this is actually CAS no. 2 of Figure 3.

The effect of electron correlation on the PE profile of the $^1\pi\pi^*$ state of MA along the R_- reaction coordinate is shown in Figure 4. The CASSCF and CASPT2 calculations were performed at the geometries optimized at the CASSCF/6-31G** level with the medium active space. For all PE profiles in Figure 4 the energy at $R_- = 0$ is defined as the zero of the energy scale. One can see that the CASSCF approximation with the small active space predicts a barrier for the PT reaction as discussed above (cf. Figure 3). The CASPT2 correction calculated with respect to the small-active-space CASSCF wave function restores the single minimum at the symmetrical configuration (Figure 4a). The CASPT2 correction apparently overestimates stabilization of the C_{2v} structure, as reflected by the rather steep rise of the PE function vs the R_- coordinate. With increasing size of the active space (medium and extended) the CASSCF and the CASPT2 PE functions converge successively toward each other (Figure 4b and c, respectively). This remarkable result leads to the conclusion that the CASSCF approximation with the medium active space already provides a qualitatively correct description of the PE profile in the $^1\pi\pi^*$ state of MA. The medium active space is used hereafter in the CASSCF calculations if not specified otherwise.

The dipole moments of the ground and the excited singlet states were calculated from the CASSCF wave functions with the medium active space. The oscillator strengths for the absorption from the ground state were calculated using CASSCF (extended CAS) transition dipole moments and CASPT2 energies.

3. Results of Calculations

3.1. Hydrogen Transfer. *A. Reaction Path.* The minimum-energy-path PE profiles of the ground and the two lowest excited singlet states of MA calculated with the medium active space as a function of the PT reaction coordinate (R_-) are shown in Figure 5a. The ordering of the excited singlet states, $E(^1n\pi^*) < E(^1\pi\pi^*)$, is in agreement with experimental observations.[29] The S_0 and S_1 ($n\pi^*$) PE functions exhibit barriers of about 2200 and 9900 cm^{-1}, respectively, at this level of theory, in qualitative agreement with experiment[9] and previous calculations.[19] For the S_2 ($\pi\pi^*$) state, the present calculation predicts a minimum of the reaction-path profile at the symmetrical (C_{2v}) conformation.

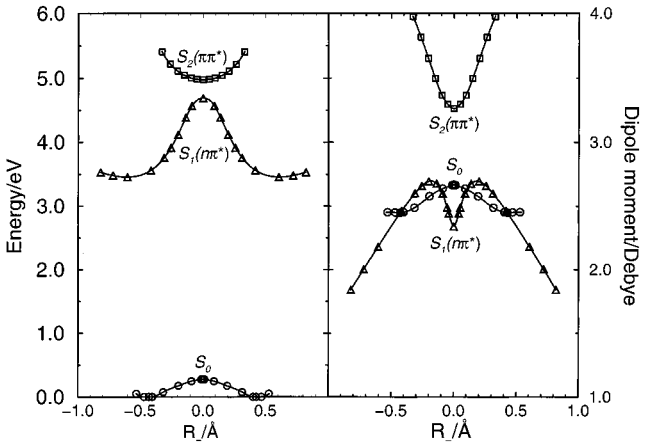

Figure 5. (a) CASSCF PE profiles and (b) dipole moments of the (circles) electronic ground state and the two lowest excited singlet states, (triangles) S_1 ($n\pi^*$) and (squares) S_2 ($\pi\pi^*$) as a function of the PT reaction coordinate R_-.

Previous calculations have been at variance with respect to the existence of a barrier for PT in the $^1\pi\pi^*$ state of MA. It has been conjectured that inclusion of electron-correlation effects causes the disappearance of the barrier found at a lower (CIS) level of theory[19] (the same effect has been conjectured for the S_1 ($n\pi^*$) state of MA). The present results provide the first direct proof of this conjecture for the S_2 ($\pi\pi^*$) state of MA, obtained at the variational CASSCF level. The effect of symmetry lowering and electron correlation on the height of the barrier of the S_1 ($n\pi^*$) and S_2 ($\pi\pi^*$) states is discussed below.

Inspection of the dipole moments presented in Figure 5b reveals that polar structures are not involved in the PT reaction in the S_0 and S_1 states, indicating that a hydrogen atom rather than a proton is transferred. The S_2 ($\pi\pi^*$) state has a significantly higher dipole moment, especially at asymmetrical configurations. The dip of the dipole moment function of the S_1 ($n\pi^*$) state at the symmetrical configuration of nuclei reflects a strong curvature of the minimum-energy reaction path near this point (vide infra). The dipole-moment functions shown in Figure 5b are of relevance for the calculation of solvent effects on the PT dynamics.

B. Structures and Vibrational Frequencies. The CASSCF-optimized geometries of the ground state and the stationary structures on the PE surfaces of the first excited singlet states of MA are presented in Figure 6. The MP2/6-31G**-optimized minimum geometry of the S_0 state is included for comparison. The analysis of these geometries leads to the conclusion that the intramolecular H-bond weakens after excitation of MA to the first excited S_1 ($n\pi^*$) state (indicated by an increase of its bond length), but gets remarkably stronger in the S_2 ($\pi\pi^*$) state. The value of $R_{OH} = 1.255$ Å in the $^1\pi\pi^*$ excited state of MA is much shorter than typical values for strongly H-bonded systems, $R_{OH} \sim 1.6$ Å. It is in fact midway between this value and that of a covalent OH bond length (~ 1.0 Å). This indicates that the strength of the bonding of the hydrogen atom to the oxygens in the $^1\pi\pi^*$ state of MA is intermediate between hydrogen-bonded and covalently bonded systems. There are also

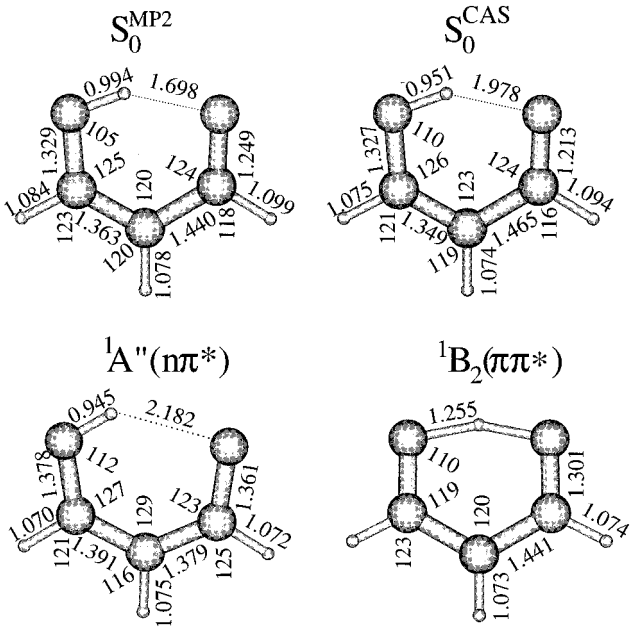

Figure 6. The MP2- and CASSCF-optimized structures at the stationary points of the PE surfaces of the ground and the lowest excited singlet states of MA. Bond lengths are in angstroms, bond angles in degrees.

noticeable variations in the bond lengths within the H-chelate ring in the different electronic states (cf. Figure 6). The electron-correlation effects beyond the CASSCF approximation reduce the H bond length and stretch the chemical bonds, as is evident from a comparison of the CASSCF- and MP2-optimized geometries of the ground state.

The stability of the structures shown in Figure 6 was checked by calculating the Hessian at the optimized geometry. The resulting sets of harmonic vibrational frequencies are presented in Table 2. One can see that the C_s-optimized structures of the S_0 and S_1 ($n\pi^*$) states represent true minima of their PE surfaces, while the C_{2v}-optimized structure of the S_2 ($\pi\pi^*$) state possesses one imaginary frequency. The vibrational mode of imaginary frequency has a_2 symmetry and essentially involves an out-of-plane motion of the meta hydrogens of the ring (out-of-plane CH mode).

The reason of this instability of the C_{2v} stationary point in the S_2 ($\pi\pi^*$) state is not clear at present. The simplest interpretation would be that it results from vibronic coupling of the $^1B_2$ ($\pi\pi^*$) state with higher lying $^1B_1$ electronic configurations, since the coupling with the lower lying $^1B_1$ ($n\pi^*$) state should increase frequencies of the a_2 modes in the $^1B_2$ ($\pi\pi^*$) state. On the other hand, one cannot exclude that this effect reflects an artifact of the single-state CASSCF approximation for the case of close-lying states.

A distortion of the molecular geometry along the a_2 vibrational mode reduces the point group from C_{2v} to C_2. In the C_2 point group both the S_1 ($n\pi^*$) and S_2 ($\pi\pi^*$) states transform according to the same (B) representation and therefore cannot be individually optimized with the CASSCF method. Reducing the molecular symmetry to C_2 and reoptimizing geometry of the lowest excited singlet state, we obtain the structure presented in Figure 7. This structure is symmetrical with respect to $R_- = 0$, but the chelate ring is noticeably skewed along the symmetry axis. The harmonic normal-mode analysis performed at this geometry yields a single imaginary frequency ($\omega = i\,638\ cm^{-1}$) reflecting PT type vibrational motion. The structure presented in Figure 7 represents the true saddle point for the PT reaction in the S_1 state of MA.

TABLE 2: Calculated Harmonic Vibrational Frequencies for Malonaldehyde-d_0 and for Malonaldehyde-d_1 in the Ground and in the First Two Excited Singlet States[a]

	S_0				$^1n\pi^*$		$^1\pi\pi^*$	
	MP2		CAS		CAS		CAS	
no.	d_0	d_1	d_0	d_1	d_0	d_1	d_0	d_1
				in-plane				
1	**276**	**268**	**261**	**282**	**204**	**201**	498	492
2	516	506	514	505	431	416	**552**	**552**
3	896	852	946	848	852	809	**864**	**728**
4	1025	1022	992	961	987	963	933	912
5	1136	1123	1181	1164	1035	1034	999	999
6	1310	1143	1360	1215	1259	1115	**1115**	**1042**
7	1439	1341	1490	1389	1300	1259	1393	**1313**
8	1442	1440	1543	1537	1415	1338	1416	1396
9	1511	1507	1584	1560	1516	1501	1516	1411
10	1684	1637	1780	1674	1529	1526	1562	1515
11	1737	1735	1888	1850	1621	1612	**1682**	**1553**
12	3088	**2417**	3150	**2990**	3358	**3035**	**1833**	1585
13	**3261**	3088	3361	3120	3395	3358	3374	3374
14	**3322**	3271	3385	3337	3417	3395	3375	3375
15	**3324**	3323	**4035**	3374	**4170**	3418	3399	3399
				out-of-plane				
16	277	278	224	229	158	142	198	198
17	373	362	395	366	313	268	273	272
18	780	684	733	572	391	378	551	547
19	895	789	810	799	491	489	647	647
20	999	965	968	941	653	640	1294	942
21	1050	1047	1077	1033	883	882	958*i*	958*i*

[a] Frequencies of vibrational modes which involve stretching of the OH/OD covalent or hydrogen bonds are printed in bold face.

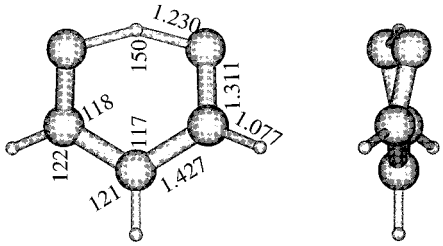

Figure 7. The CASSCF-optimized geometry of MA at the saddle point for the PT reaction in the S_1 state. Bond lengths are in angstroms, bond angles in degrees.

C. Electron-Correlation Effects beyond CASSCF. The results presented in the preceding two subsections were obtained at the CASSCF level of theory (with the medium active space as defined in Table 1). The remaining electron correlation effects may have a significant influence on the optimized geometries as well as on the vibrational frequencies, as indicated in Figure 6 and in Table 2 for the ground state. The CASPT2 method is capable of accounting for these effects in the excited electronic states, but analytic gradients are not implemented so far and thus geometry optimization and calculation of the Hessian are not possible at this level. To check the influence of the electron-correlation effects, we consider the PE profiles of the $^1n\pi^*$ and $^1\pi\pi^*$ states of MA recalculated within the CASPT2 approximation at the CASSCF/6-31G**-optimized geometries. The influence of the size of the active space as well as post-CASSCF electron-correlation effects are illustrated by comparing the calculations for the three active spaces defined in Table 1. The results of calculations for the $^1\pi\pi^*$ state have already been discussed in section 2 (Figure 4). The corresponding results for the $^1n\pi^*$ state are shown in Figure 8.

Inspecting Figure 8, one sees a noticeable reduction of the barrier for PT in the $^1n\pi^*$ state due to electron-correlation effects beyond the CASSCF approximation for all three active spaces.

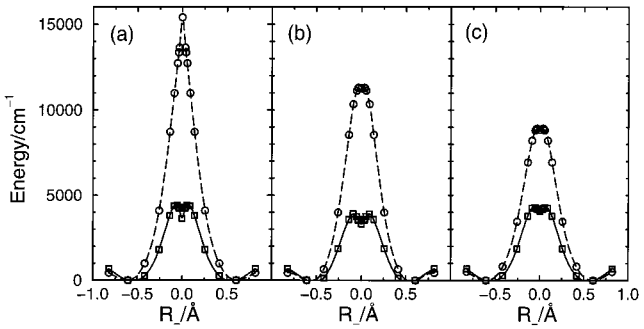

Figure 8. (circles) CASSCF and (squares) CASPT2 PE functions of the S_1 ($n\pi^*$) state of MA, calculated with the (a) small, (b) medium, and (c) extended active space as a function of the R_- reaction coordinate.

In addition, the CASPT2 PE profile in the vicinity of the minimum is more shallow than the CASSCF profile. Both effects are only weakly dependent on the size of the active space. The kink on the top of the barrier of the CASPT2 PE profile presumably reflects a strong curvature of the minimum-energy reaction path in vicinity of $R_- = 0$, as was already conjectured from the inspection of the dipole moment function of this state (Figure 5b). The depth of the kink seems to decrease with increasing size of the active space, but it is still present even for the most extended active space used in the calculations (Figure 8c).

Generally, the electron-correlation effects on the PE profile of the S_1 ($n\pi^*$) state along the R_- coordinate are similar to those observed for the ground state (when one compares the MP2 results with those obtained at the CASSCF level). The electron-correlation effects reduce the barrier for PT in the S_1 ($n\pi^*$) state and thus decrease the frequency of the OH stretching vibration. Both effects can hardly be recovered by increasing the active space in the CASSCF calculations, as is seen from inspection of Figure 8a−c. Correlation effects reduce the barrier for the PT reaction in the S_1 ($n\pi^*$) state, but the barrier remains significant even for the largest active space used in the calculations. There is thus a qualitative difference between the electron-correlation effects on the PE profiles of the S_1 ($n\pi^*$) and S_2 ($\pi\pi^*$) states: for the latter, saturation of the effects could be obtained already at the CASSCF level, while inclusion of post-CASSCF correlation effects is essential for the former.

In Figure 9 and in Table 3 we present the energy-level scheme of MA calculated within the CASPT2 approximation (extended CAS) at the geometries optimized at the CASSCF/6-31G** level for the excited states and at the MP2/6-31G** level for the ground state. The CASPT2 barrier for PT in the ground state, 0.136 eV (1100 cm^{-1}), is slightly lower than the MP2/6-31G** barrier (1200 cm^{-1}).[11−13] The C_{2v}-constrained minimum of the $^1B_2$ ($\pi\pi^*$) state is almost degenerate with the energy of the transition state in the $^1B_1$ ($n\pi^*$) state. Both states are thus expected to be strongly coupled by vibrational modes of a_2 symmetry. This coupling stabilizes the energy of the transition state in the S_1 state by about 1000 cm^{-1} due to symmetry lowering from C_{2v} to C_2. Comparing the energy of the transition structure (the saddle point for the PT reaction) with the minimum of the S_1 ($n\pi^*$) state, one can estimate the barrier for the PT reaction in this state to be about 0.38 eV (3000 cm^{-1}). This is larger than the barrier predicted for the ground state by nearly a factor of 3.

The fluorescence from the S_1 ($n\pi^*$) state (the maximum of the band) is predicted to occur at about 2.72 eV. It is significantly shifted with respect to the 0−0 line predicted for this transition (about 3.38 eV) and reflects a strong rearrangement of the molecular geometry between these states. The

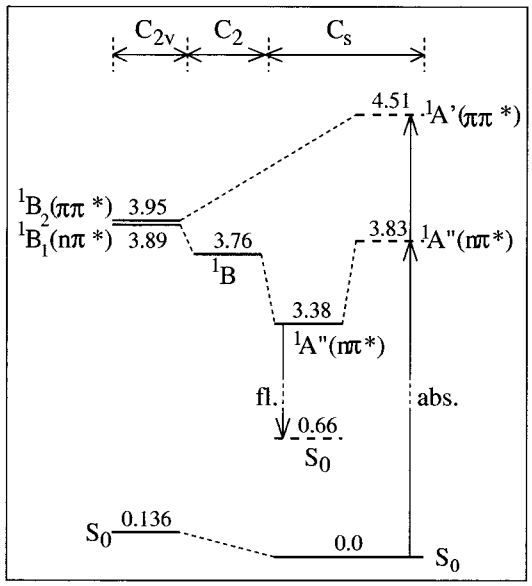

Figure 9. The energy-level scheme relevant for the optical spectroscopy of MA, calculated at MP2 (ground state) and CASSCF (excited states) optimized geometries (solid lines). Dashed lines denote vertical energy calculated at geometry as indicated by arrow. Numbers denote CASPT2 energy (in eV) with respect to the minimum of the ground state.

vertical excitation energies (calculated at the MP2/6-31G** geometry) of the S_1 ($n\pi^*$) and S_2 ($\pi\pi^*$) states are predicted to be 3.83 and 4.51 eV, respectively. The oscillator strengths for these transitions obtained with the use of the CASSCF (extended active space) transition dipole moments and the CASPT2 energies are 1×10^{-4} and 0.244 for the S_1 ($n\pi^*$) and S_2 ($\pi\pi^*$) states, respectively.

3.2. Hydrogen Detachment. *A. Reaction Path.* Before presenting the results of the calculations, we discuss briefly the electronic configurations which are expected to be relevant for this process. The electronic wave functions of the lowest excited singlet states of MA, B_1 ($n\pi^*$), and B_2 ($\pi\pi^*$), are dominated by the electronic configurations b_2 (n) a_2 (π^*) and b_1 (π) a_2 (π^*), respectively, when the molecular symmetry is restricted to the C_{2v} point group (Figure 10). Detachment of the hydrogen atom involves the breaking of the OH bond(s) and thus the σ^* orbital which has nodes at these bond(s) is expected to be lowered in energy with increasing R_+ coordinate. The variation of the energy of the most relevant molecular orbitals along the R_+ coordinate is schematically illustrated in Figure 11 (canonical HF energies in the S_0 state). It can be seen that the electronic configurations b_2 (n) a_1 (σ^*) and b_1 (π) a_1 (σ^*) of B_2 and B_1 symmetry, respectively, are expected to be important for the description of the PD reaction.

The CASSCF (medium CAS) PE profiles of the ground and the lowest excited singlet states of B_2 and B_1 symmetry of MA plotted vs the R_+ reaction coordinate are shown in Figure 12a. The PEs of both the B_1 ($n\pi^*$) and B_2 ($\pi\pi^*$) excited singlet states and the ground-state rise with increasing OH distance. The B_2 ($n\sigma^*$) and B_1 ($\pi\sigma^*$) excited singlet states are much higher in energy for R_+ values in vicinity of the minima of the "locally" excited states, but their energies decrease strongly upon stretching of the OH distance. The B_2 ($n\sigma^*$) and B_1 ($\pi\sigma^*$) states are seen to intersect the "locally" excited singlet states as well as the ground state. The extremely weak interaction between the $^1n\pi^*$ and $^1\pi\sigma^*$ as well as the $^1\pi\pi^*$ and $^1n\sigma^*$ electronic configurations of the same symmetry in the C_{2v} point group (difference in occupation of two orbitals) allows us to individu-

TABLE 3: CASSCF and CASPT2 Energies (in au), Dipole Moments μ (in Debye), Weights of the CASSCF Reference Function in the First-Order Wave Function (ω), and Energies Relative to the Minimum of the Ground State ΔE (in eV), Calculated with the ANO-L(3s2p1d/2s1p) Basis Set at the Stationary Points on the PE Surfaces of the Ground and the Two Lowest Excited Singlet States of Malonaldehyde

geometry	state	E_{CASSCF}	ΔE_{CASSCF}	μ	E_{CASPT2}	ω	ΔE_{CASPT2}
$S_0(C_s)^a$	S_0	−265.883 83		2.630	−266.495 25	0.840	
	$S_1(n\pi^*)$	−265.709 52	4.741	1.849	−266.354 63	0.823	3.825
	$S_2(\pi\pi^*)$	−265.669 21	5.838	4.090	−266.329 57	0.810	4.507
$S_0(C_{2v})^a$	S_0^{TS}	−265.877 53	0.171	2.979	−266.490 23	0.841	0.136
$S_1(C_s)^b$	S_0	−265.858 33	0.694	3.051	−266.471 09	0.837	0.657
	$S_1(n\pi^*)$	−265.737 98	3.967	1.689	−266.370 86	0.829	3.383
$S_1(C_2)^b$	S_1^{TS}	−265.700 49	5.065	2.893	−266.356 98	0.811	3.761
$S_1(C_{2v})^b$	$S_1(n\pi^*)$	−265.697 61	4.987	1.788	−266.352 30	0.821	3.888
$S_2(C_{2v})^b$	$S_2(\pi\pi^*)$	−265.693 17	5.186	3.101	−266.349 94	0.811	3.952

[a] MP2/6-31G**-optimized geometry. [b] CASSCF/6-31G**-optimized geometry.

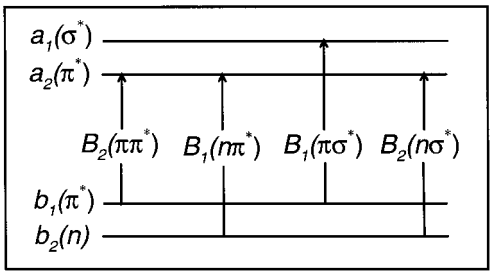

Figure 10. The frontier orbitals of MA with C_{2v} symmetry labels and the electronic terms associated with the promotion of one electron between these orbitals.

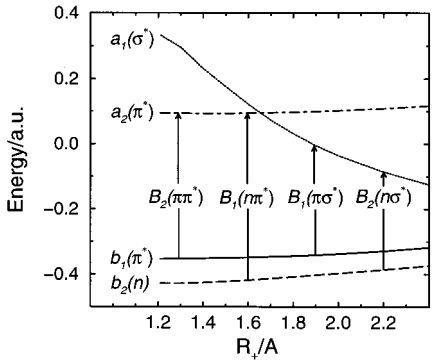

Figure 11. Variation of the canonical HF orbital energies of the "frontier" orbitals of Figure 10 vs the R_+ coordinate.

ally optimize these states within some range of the R_+ coordinate. Both electronic configurations involving excitations to the σ^* orbital (particularly the $^1\pi\sigma^*$ configuration) are more polar than the ground and the "locally" excited singlet states. (Figure 12b).

The intersections between the B_1 and B_2 states develop into conical intersections when out-of-plane displacements of a_2 symmetry are taken into account. This produces a barrier on the PE surface of the S_1 state with respect to the PD reaction (full squares in Figure 12a). The intersections of the B_1 ($\pi\sigma^*$) and B_2 ($n\sigma^*$) states with the ground state give rise to conical intersections when the molecular frame is distorted along coordinates of b_1 (out-of-plane) and b_2 (in-plane) symmetry, respectively. The energetically lowest intersection between the S_0 and the B_1 ($\pi\sigma^*$) states gives rise to a barrier on the PE surface of the S_0 state with respect to the PD reaction (full circles in Figure 12a). The geometries of the transition states corresponding to the tops of these barriers in the S_0 and S_1 states are presented in Figure 13.

The effect of vibronic mixing of the C_{2v}-optimized electronic states also is evident from inspection of the dipole-moment

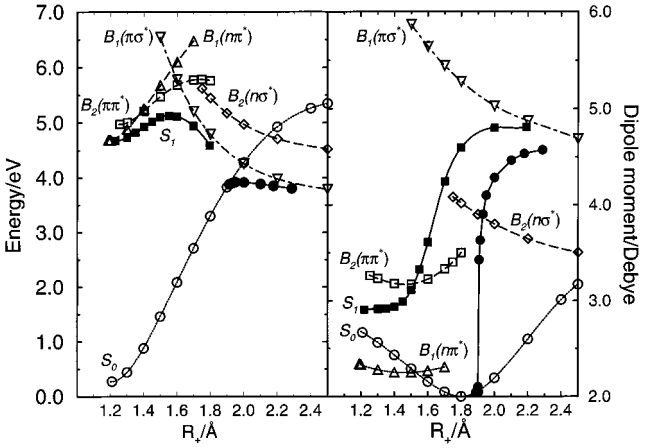

Figure 12. (a) CASSCF PE profiles and (b) dipole moments of the electronic ground state (circles) and the two lowest locally excited, $n\pi^*$ (triangles up) and $\pi\pi^*$ (squares), and dissociative excited, $\pi\sigma^*$ (triangles down) and $n\sigma^*$ (diamonds), singlet states of B_1 and B_2 symmetry in the C_{2v} point group as a function of the PD reaction coordinate R_+. The solid curves refer to reaction paths in the S_0 (dots) and in the S_1 (solid squares) states, optimized with C_s' and C_2 symmetry constraint, respectively.

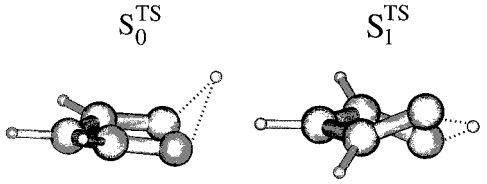

Figure 13. Geometries of the barriers with respect to R_+ in the S_0 and S_1 states of MA.

functions shown in Figure 12b. The dipole moment of the ground state shows an abrupt rise within a narrow range of R_+ between the C_{2v}-calculated values for the S_0 and the B_1 ($\pi\sigma^*$) states following the minimum-energy path of C_s' symmetry (with symmetry plane perpendicular to the molecular plane). The dipole moment of the S_1 state calculated at its C_2 minimum indicates a "fifty-fifty" mixing of the $^1n\pi^*$ and $^1\pi\pi^*$ configurations. The dipole-moment rises abruptly with increasing OH distance up to the value determined for the B_1 ($\pi\sigma^*$) state along the C_2-optimized minimum-energy path.

B. Electron-Correlation Effects beyond CASSCF. In analogy to the preceding section, the influence of electron-correlation effects on the CASSCF-calculated PE profiles along the R_+ reaction coordinate was checked by calculating the CASPT2 energies at the CASSCF-optimized geometries. We consider the effect of electron correlation on the PE profile of the S_2 ($\pi\pi^*$) state which provides an estimate of the correlation effects on

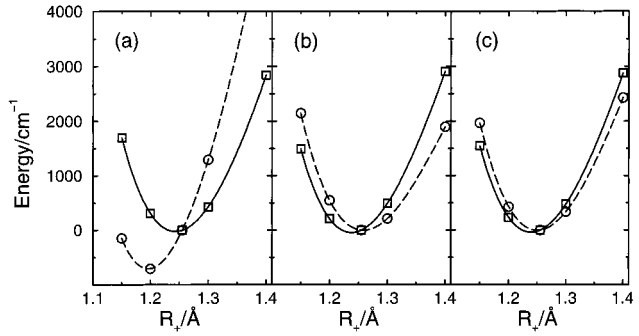

Figure 14. (circles) CASSCF and (squares) CASPT2 PE functions of the S_2 ($\pi\pi^*$) state of MA, calculated with the (a) small, (b) medium, and (c) extended active space vs the R_+ reaction coordinate. The energy at $R_+ = 1.25$ Å (minimum of the $\pi\pi^*$ state) defines the zero of the energy scale.

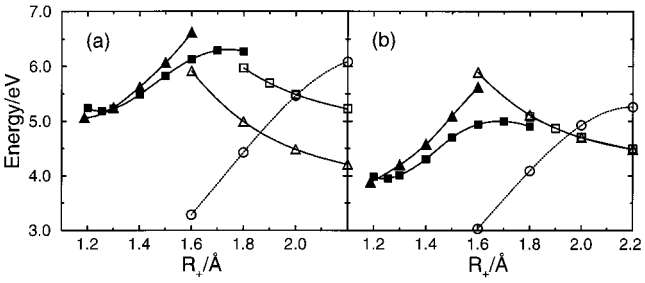

Figure 15. (a) CASSCF and (b) CASPT2 PE functions of the (circles) ground, the (solid triangles) "locally" excited $^1B_1$ ($n\pi^*$), and (solid squares) $^1B_2$ ($\pi\pi^*$) and the (squares) "dissociative" $^1B_2$ ($n\sigma^*$) and (triangles) $^1B_1$ ($\pi\sigma^*$) states, calculated along the hydrogen-detachment reaction coordinate.

the vibrational frequencies of this state. The S_1 ($n\pi^*$) state was not considered in this study since the C_{2v} geometry represents a transition structure with respect to the PT reaction on the PE surface of this state.

The results are presented in Figure 14. One sees that with exception of the small active space (Figure 14a), the CASSCF and the CASPT2 PE profiles (obtained with the medium and extended CAS) are similar in shape. The CASPT2 minimum is shifted to a somewhat smaller value of the R_+ coordinate than the CASSCF minimum. More pronounced differences between the CASSCF and CASPT2 results were found in the "photochemical" range of the R_+ reaction coordinate (Figure 15). The comparison of Figure 15a and b reveals that the electron-correlation effects beyond CASSCF are remarkably different for different electronic configurations. The "locally" excited B_1 ($n\pi^*$) and B_2 ($\pi\pi^*$) singlet states are stabilized by a similar amount but noticeably more than the B_2 ($n\sigma^*$) and B_1 ($\pi\sigma^*$) states. Moreover, the CASPT2-corrected PE profiles of the latter two states are degenerate to a very good approximation. This is an astonishing result at the first glance, considering the very different orbital nature and geometries of these states. The similar slopes of the CASPT2 (and also CASSCF) PE profiles can be explained by the fact that the $10a_1$ (σ^*) orbital does not overlap with the $7b_2$ (n) and $2b_1$ (π) orbitals due to the different symmetry. Thus the PE profiles of the B_2 ($n\sigma^*$) and B_1 ($\pi\sigma^*$) states are determined by the interaction of the electron residing on the $10a_1$ (σ^*) orbital localized on the detached hydrogen atom with the same doubly occupied core. The explanation of the apparent degeneracy of the $n\sigma^*$ and $\pi\sigma^*$ CASPT2 PE profiles (see Figure 15b) is more involved. To shed some light on this problem, we have optimized the remaining radical (after removal of the hydrogen atom) in the $^2B_2$ (n) and $^2B_1$ (π) states. The resulting geometries are very similar to geometries of the molecular ring optimized along the R_+ coordinate in the B_2 ($n\sigma^*$) and B_1 ($\pi\sigma^*$) states, respectively. The CASSCF energies (extended CAS) of these doublets differ by about 1 eV, but this splitting is reduced to only 200 cm^{-1} at the CASPT2 level in agreement with the results shown in Figure 15. Thus the degeneracy of the CASPT2 PE profiles of the B_2 ($n\sigma^*$) and B_1 ($\pi\sigma^*$) states of MA seems to be accidental.

4. Discussion of Results

4.1. Technical Aspects. Before we discuss the implications of the results obtained in this work for the spectroscopy and photophysics of MA, we discuss briefly some methodological aspects resulting from our study. As discussed in section 2 (Figures 3 and 4), the proper selection of the active space for the CASSCF calculations is the key point for a qualitatively correct description of the PT reaction in the $^1\pi\pi^*$ state. A correct description can be achieved if apart from the π orbitals also some frontier σ orbitals are included into the active space. Our results clearly show that at least a pair (σ and σ^*) of such orbitals has to be included into the active space in order to recover important nondynamical $\pi\sigma$ and $\sigma\sigma$ electron correlation effects. If the σ orbitals are not included into the active space, the single-minimum character of the $^1\pi\pi^*$ state can only be reproduced at a higher level of theory like CASPT2.

Let us mention in this context that the vanishing of the CASSCF-calculated barrier for the PT reaction on the PE surface of the S_1 ($\pi\pi^*$) at the CASPT2 level has already been found for the larger proton-transferring systems *o*-hydroxybenzaldehyde (OHBA)[30] and salicylic acid (SA).[31] In both cases the active space used in the CASSCF calculations was limited to the π orbitals only, corresponding to the small CAS defined above for MA. The results of the present study clearly indicate that the CASSCF approximation with an active space composed of the π orbitals only cannot provide a qualitatively correct description of the PT reaction profile in the $^1\pi\pi^*$ state. Moreover, since not dynamical electron correlation but orbital relaxation is responsible for the effect, the CASPT2 method does not work properly when applied with a π only active space. This represents a true bottleneck for the application of the method to larger proton-transferring systems. This problem needs further investigations, but the strategy which follows from the present study is clear: one has to select a compact active space for the CASSCF calculations by including properly localized σ orbitals (possibly at the expense of eliminating some less important π orbitals in larger systems) in order to handle as much as possible the nondynamical $\pi\sigma$ and $\sigma\sigma$ relaxation effects at the variational level.

4.2. Spectroscopy of the S_1 ($n\pi^*$) State of MA. So far only the S_0 and S_1 ($n\pi^*$) states of MA have been the subject of detailed spectroscopic investigations. Apart from the absorption spectrum, the S_2 ($\pi\pi^*$) state has not been amenable to direct spectroscopic observations since the spectrum is diffuse and the state is nonfluorescent. The ground state of MA is not of particular interest here, since its PE surface has already been extensively explored at different levels of theory[10−13] and tunneling splittings and vibrational energy levels have been calculated.[12,14−17] The S_1 ($n\pi^*$) state is the state of primary interest in this work with respect to the spectroscopy of MA.

We have shown that the S_1 ($n\pi^*$) transition state has C_2 symmetry, while the minimum has C_s symmetry. At the C_s-minimum of the S_1 ($n\pi^*$) state all vibrational frequencies are real (see Table 2), while a single imaginary frequency of 638 cm^{-1} was found at the transition state. The vibrational motion

along the normal mode of imaginary frequency essentially involves the PT coordinate R_-. The barrier which separates the two equivalent minima on the PE surface of the S_1 ($n\pi^*$) state was estimated at the CASPT2 level to be about 3000 cm^{-1} (cf. Figure 9 and Table 3). Our results confirm the experimental conclusion that there is a significant barrier on the S_1 ($n\pi^*$) surface with respect to the PT reaction,[18] noticeably higher than the barrier in the ground state.

The CASSCF geometries of the S_0 and S_1 states (Figure 6) differ substantially in many internal coordinates. This finding is consistent with the long vibronic progressions observed in the $S_0 \rightarrow S_1$ absorption spectrum of MA.[18,32] Scaling the CASSCF vibrational frequencies in the S_1 state by the factor 0.96 determined from the ratio of MP2 and CASSCF ground-state frequencies (excluding the CH and OH stretching modes), we are able to support the assignment of the progression-forming modes 185 and 1300 cm^{-1} to ring bending and carbonyl stretching, respectively.[18]

Our CASPT2 prediction of the energy of the 0−0 line for the transition between the S_0 and S_1 ($n\pi^*$) states (3.38 eV) is lower by 0.12 eV than the experimental value.[18] This difference is within the expected accuracy of the CASPT2 method for systems of such size.[22] Our calculations predict a substantial difference between the 0−0 line and the vertical energies of absorption (3.89 eV) and fluorescence (2.72 eV). Thus a substantial Stokes shift between the absorption and fluorescence maxima of about 9000 cm^{-1} is predicted. The CASSCF-calculated oscillator strength for the dipole transition between the S_0 and S_1 states is of the order of 10^{-4}. This indicates that fluorescence from the S_1 ($n\pi^*$) state of MA is extremely weak due to the expected competition of intersystem crossing to the $^3\pi\pi^*$ state.

4.3. Remarks on the $^1\pi\pi^*$ State. The calculated maximum and oscillator strength of the S_2 ($\pi\pi^*$) absorption band are $\nu_{theor} = 4.51$ eV and $f_{theor} = 0.224$, respectively. The corresponding experimental values are: $\nu_{exp} \simeq 4.7$ eV and $f_{exp} \simeq 0.3$.[29] The deviation of about 0.2 eV is within the expected accuracy of the CASPT2 method but again indicates that the CASPT2 approximation overstabilizes the S_2 ($\pi\pi^*$) state relative to the ground state.

The qualitatively different feature of the $^1\pi\pi^*$ state of MA compared to the S_0 and $^1n\pi^*$ states is its single minimum at the symmetrical C_{2v} configuration. This result has been for the first time obtained here for a proton-transferring system at the variational (CASSCF) level. Our extensive study presented in section 3.1 has clearly shown that this result is not an artifact of the theoretical approximations. The Hessian determined at the C_{2v} geometry within the CASSCF approximation is expected to be converged with respect to electron correlation effects. This provides us with the opportunity to perform a normal-mode analysis at the stationary geometries of the $^1\pi\pi^*$ state.

One has to keep in mind that the C_{2v} stationary geometry of the $^1B_2$ ($\pi\pi^*$) state represents, in the CASSCF approximation, a saddle-point with respect to out-of-plane deformation of the ring (cf. imaginary frequency in Table 2). It cannot be excluded at present that this instability reflects an artifact of the single-state CASSCF approximation. Otherwise, it obviously results from vibronic coupling between the close lying $^1\pi\pi^*$ and $^1n\pi^*$ states of MA. Only vibrational modes of a_2 symmetry can be involved in the coupling. None of these modes involve vibrational motion of the "mobile" hydrogen atom. Thus the most characteristic feature of the vibrational spectrum of the $^1\pi\pi^*$ state (Table 2), namely, the strong coupling of the hydrogen motion to the ring in-plane modes due to the conjugation within the H-chelate ring, is unaffected by the out-of-plane deformation.

The vibrational frequencies of the modes which involve stretching of the OH/OD covalent and hydrogen bonds are indicated in Table 2 in bold face. One sees that the O−H/O−D (and O···H/O···D) stretch modes are clearly separated from the other modes in the S_0 and S_1 ($n\pi^*$) states. The effect of electron correlation included for the ground state at the MP2 level causes a mixing of the OH stretching mode only with the CH stretching modes of similar frequencies. The situation is qualitatively different in the $^1\pi\pi^*$ state. There an admixture of the OH/OD stretching motion spreads over the whole vibrational spectrum with a noticeable absence of a typical high-frequency O−H/O−D stretching mode as well as low-frequency O···H/O···D stretching (chelate ring bending) modes. The highest frequency vibrational mode which involves the OH stretch is the 1833 cm^{-1} symmetric stretching mode (R_+ coordinate). The frequency of this mode is reduced to 1313 cm^{-1} upon deuterium substitution. The highest frequency mode which involves asymmetric stretch of the OH/OD bonds (R_- coordinate), nominally a CO stretching mode, has the frequency 1682/1553 cm^{-1}, while the lowest one, nominally a CC stretching mode, has a frequency of only 863/728 cm^{-1}. The 522 cm^{-1} mode which is invariant to deuterium substitution involves the symmetrical stretch of the two OH bonds due to ring opening, the hydrogen atom remaining stationary. The 1115/1042 cm^{-1} mode consists of a mixture of the asymmetric OH/OD stretching motion and the CCH bending motion.

The vibrational motion in the $^1\pi\pi^*$ state of MA clearly reflects a strong conjugation within the H-chelate ring (pseudo-aromaticity), an effect which is absent in both the S_0 and S_1 ($n\pi^*$) states. The drastic difference between the vibrational force fields in the ground and in the $^1\pi\pi^*$ state, together with a significant difference of equilibrium geometries, can explain the loss of any similarity of the $S_0-{}^1\pi\pi^*$ absorption and emission spectra. This effect cannot directly be observed in MA because of the presence of the close-lying S_1 ($n\pi^*$) state. The $^1\pi\pi^*$ state, however, becomes the first excited singlet state in larger PT systems. Theoretical results obtained at the CASPT2 level indicate that this already is the case for OHBA and for SA and that the PE profile of the S_1 ($\pi\pi^*$) state in these systems exhibits a single minimum with respect to the PT reaction.[30,31]

The H chelate ring of MA represents the reaction center of these as well as larger systems and our predictions resulting from the normal-mode analysis performed in the $^1\pi\pi^*$ state of MA can in a natural way explain some of the peculiarities of the spectra observed in jet-cooled SA[33] and 1-hydroxy-2-acetonaphthone (HAN),[34] for example. The vibronic structure of the dispersed fluorescence spectra of these compounds is completely unrelated to the vibronic structure of the fluorescence excitation spectra. Moreover, there is a remarkable difference between the dispersed fluorescence spectra obtained for excitation of the origin of the S_0-S_1 ($\pi\pi^*$) transition and strong vibronic lines in the excitation spectrum (849 cm^{-1} for SA[33] and 836 cm^{-1} for HAN[34]). The energies of these vibronic lines are close to the lowest frequency which involves the asymmetric OH stretching motion in the $^1\pi\pi^*$ state of MA (863 cm^{-1}). Dushinsky rotation and the shift in equilibrium geometry are expected to induce vibronic progressions in many vibrational modes of the ground state, an effect which is indeed observed in the dispersed fluorescence spectra of these systems.

4.4. Photophysics of MA. The mechanism which is expected to govern the photophysics of MA excited with some excess of

energy above the origin of the S_1 state is the access to an efficient nonradiative channel provided by the hydrogen-detachment reaction, see Figure 12a. We have estimated a barrier of about 1 eV for this process on the PE surface of the S_1 state at the CASPT2 level, see Figure 15b. This estimate is not finally conclusive in view of the significant difference between the variational CASSCF (Figure 15a) and perturbational CASPT2 (Figure 15b) predictions. Moreover, there are strong indications that CASPT2 underestimates the excitation energies of the "locally" excited states as discussed above. Nevertheless, the existence of the PD channel and its potential importance for the photophysics of MA are clearly demonstrated by our results.

The existence of such a "dissociative" PE profile is not surprising in itself. One can expect similar PE functions along any intramolecular coordinate that breaks a chemical bond. The special feature of the B_1 ($\pi\sigma^*$) and B_2 ($n\sigma^*$) PE profiles presented in Figures 12 and 15 is their intersection with the ground state along the R_+ coordinate. These intersections are symmetry-allowed within the C_{2v} point group and are converted into conical intersections by distortions of the molecular geometry along vibrational modes of b_1 and b_2 symmetry, respectively. Thus the $^1n\sigma^*$ state couples to the ground state via in-plane displacements which reduce the C_{2v} symmetry to C_s, while the $^1\pi\sigma^*$ state couples via out-of-plane distortions of the type presented in Figure 13. The question which of the PE surfaces, $^1n\sigma^*$ or $^1\pi\sigma^*$, is more relevant for the relaxation dynamics of MA cannot definitively be answered at the present stage. In any case, the cones they form at the intersection with the ground state can provide the mechanism for very efficient internal conversion.[35] Let us note that the apparent intersections of the PE functions in Figures 12 and 15 are not the real intersections, since the PE functions were optimized for each electronic state separately.

It is very likely that the mechanism of internal conversion sketched above dominates the photophysics of MA. It has been shown that prolonged (4 h) UV irradiation of MA isolated in a xenon matrix does not lead to any other photochemistry than rotamerization.[36,37] In this experiment MA was excited to the $^1\pi\pi^*$ state with a broad-band mercury lamp ($\lambda > 230$ nm). The accumulated experimental data (for a review see ref 38) show that rotamerization and ketonization are the most abundant photoreactions in a wide class of β-dicarbonyl compounds excited within the 250−300 nm region of the first $\pi \rightarrow \pi^*$ singlet transition. Moreover, excitation within this band is ineffective in giving rise to luminescence. Thus, the radiationless processes associated with the photoreactions of these compounds are fast enough to compete with relaxation to the lower lying $^1n\pi^*$ states. The spectral changes caused by UV irradiation are reversible, i.e., the original solution spectra are restored in the dark.[39] The presence of a ring system in β-dicarbonyl compounds reduces considerably the yield of photoconversion due to hindering of some intramolecular rotations within the H-chelate ring, but still the radiationless decay to the ground state dominates the photophysics. These compounds show, therefore, remarkable stability against degradation caused by UV radiation.[1]

The experimental data on the photophysics of the H-chelate-ring systems discussed above point to the conclusion that the photoisomerization of these compounds proceeds by an efficient radiationless process which takes place after excitation to the lowest excited $^1\pi\pi^*$ state. The authors of ref 37 comment that excitation within the S_1 ($n\pi^*$) state does not lead to isomerization of the molecule. If it is impossible to break a relatively weak (as indicated by our results) hydrogen bond in the $^1n\pi^*$ state, rotamerization due to excitation to the much more strongly H-bonded $^1\pi\pi^*$ state seems to be even less likely. The proton detachment/attachment process, on the other hand, can explain this radiationless process, the threshold of which lies within the absorption band of the $^1\pi\pi^*$ state. The hydrogen bond is broken in the course of the PD reaction and the ring fragment therefore can easily rotate. The structure optimized at the top of the barrier in the ground state (Figure 13) may represent the transition state for the ketonization reaction. When intramolecular rotations are hindered by chemical substitutions, the PD reaction just provides an efficient mechanism for internal conversion to the ground state.

5. Conclusions

A brief summary of the results of the present work can be given as follows.

(**i**) The barrier for the PT reaction in the S_1 ($n\pi^*$) state is about 3000 cm^{-1} and is significantly larger than the barrier in the ground state. The H-bond in the S_1 ($n\pi^*$) state is weaker than the H-bond in the ground state.

(**ii**) The S_2 ($\pi\pi^*$) state exhibits a barrierless single-minimum PE profile for the PT reaction, reflecting a significantly stronger H-bond than in the ground state. The strong H-bond in the S_2 ($\pi\pi^*$) state results from a pronounced conjugation (pseudo-aromaticity) within the H chelate ring. As a consequence, the vibrational dynamics in the S_2 ($\pi\pi^*$) state differs drastically from the vibrational dynamics in the S_0 and S_1 ($n\pi^*$) states.

(**iii**) As a function of the in-plane symmetric hydrogen-detachment coordinate, the PE profiles of the S_0, S_1 ($n\pi^*$), and S_2 ($\pi\pi^*$) states are crossed by the PE curves of repulsive $^1\pi\sigma^*$ and $^1n\sigma^*$ states. The associated multiple conical intersections presumably provide the mechanism for efficient radiationless decay from the excited singlet states to the ground state. The threshold for this photophysical process is predicted to be located within the S_2 ($\pi\pi^*$) absorption band.

(**iv**) We suggest that the understanding of the mechanistic details of the photochemistry of MA may provide the key for the rationalization of the complex photochemical behavior of larger proton-transferring systems and β-dicarbonyl compounds, which contain the H-chelate ring of MA. The photochemical mechanisms revealed by the present study of MA naturally explain that rotamerization and ketonization prevail in single-ring systems, while radiationless decay to the ground state will dominate in systems containing aromatic rings.

Acknowledgment. This work has been supported by the Deutsche Forschungsgemeinschaft by a guest professorship for A.L.S.

References and Notes

(1) Heller, H. J.; Blattmann, H. R. *Pure Appl. Chem.* **1974**, *36*, 141.
(2) Formosinho, S. J.; Arnaut, L. G. *J. Photochem. Photobiol. A* **1993**, *75*, 21.
(3) Douhal, A.; Lahmani, F.; Zewail, A. H. *Chem. Phys.* **1996**, *207*, 477.
(4) Perrin, C. L.; Nielson, J. B. *Annu. Rev. Phys. Chem.* **1997**, *48*, 511.
(5) de la Vega, J. R. *Acc. Chem. Res.* **1982**, *15*, 185.
(6) Rowe, W. F., Jr.; Duerst, R. W.; Wilson, E. B. *J. Am. Chem. Soc.* **1976**, *98*, 4021.
(7) Baughcum, S. L.; Duerst, R. W.; Rowe, W. F.; Smith, Z.; Wilson, E. B. *J. Am. Chem. Soc.* **1981**, *103*, 6296.
(8) Turner, P.; Baughcum, S. L.; Coy, S. L.; Smith, Z. *J. Am. Chem. Soc.* **1984**, *106*, 2265.
(9) Baughcum, S. L.; Smith, Z.; Wilson, E. B.; Duerst, R. W. *J. Am. Chem. Soc.* **1984**, *106*, 2260.
(10) Fluder, E. C.; de la Vega, J. R. *J. Am. Chem. Soc.* **1978**, *100*, 5265.
(11) Frisch, M. J.; Scheiner, A. C.; Schaefer, H. F., III; Binkley, J. S. *J. Chem. Phys.* **1985**, *82*, 4194.

(12) Shida, N.; Barbara, P. F.; Almlöf, J. E. *J. Chem. Phys*. **1989**, *91*, 4061.
(13) Barone, V.; Adamo, C. *J. Chem. Phys*. **1996**, *105*, 11007.
(14) Carrington, T., Jr.; Miller, W. H. *J. Chem. Phys.* **1986**, *84*, 4364.
(15) Chiavassa, T.; Roubin, P.; Pizzala, L.; Verlaques, P.; Allouche, A.; Marinelli, F. *J. Phys. Chem.* **1992**, *96*, 10659.
(16) Binkley, J. S.; Frisch, M. J.; Schaefer, H. F., III *Chem. Phys. Lett*. **1986**, *126*, 1.
(17) Tayyari, S. F.; Milani-Nejad, F. *Spectrochim. Acta A* **1998**, *54*, 255.
(18) Seliskar, C. J.; Hoffman, R. E. *J. Mol. Spectrosc*. **1981**, *88*, 30.
(19) Luth, K.; Scheiner, S. *J. Phys. Chem*. **1994**, *98*, 3582.
(20) Arias, A. A.; Wasserman, T. A. W.; Vaccaro, P. H. *J. Chem. Phys*. **1997**, *107*, 5617.
(21) Roos, B. O. *Adv. Quantum Chem.* **1987**, *69*, 399.
(22) Andersson, K.; Roos, B. O. In *Modern Electronic Structure Theory*; Yarkony, D. R., Ed.; World Scientific: 1995; p 55−109.
(23) Sobolewski, A. L.; Domcke, W. *Chem. Phys. Lett*. **1999**, *300*, 533.
(24) Schmidt, M. W.; Baldridge, K. K.; Boatz, J. A.; Elbert, S. T.; Gordon, M. S.; J., Jensen, H.; Koseki, S.; Matsunaga, N.; Nguyen, K. A.; Su, S. J.; Windus, T. L.; Dupuis, M.; Montgomery, J. A. *J. Comput. Chem*. **1993**, *14*, 1347.
(25) Frisch, M. J.; et al. *GAUSSIAN 94*, Revisions B.3 and D.4; Gaussian, Inc.: Pittsburgh, PA, 1994.
(26) Binkley, J. S.; Pople, J. A.; Hehre, W. J. *J. Am. Chem. Soc*. **1980**, *102*, 939. Gordon, M. S.; Binkley, J. S.; Pople, J. A.; Pietro, W. J.; Hehre, W. J. *J. Am. Chem. Soc.* **1982**, *104*, 2797.
(27) Schmidt, M. W.; Gordon, M. S. *Annu. Rev. Phys. Chem*. **1998**, *49*, 233.
(28) Andersson, K.; et al. *MOLCAS, Version 4, User's Guide*; University of Lund: Sweden, 1997.
(29) Seliskar, C. J.; Hoffman, R. E. *Chem. Phys. Lett.* **1976**, *43*, 481.
(30) Sobolewski, A. L.; Domcke, W. *Chem. Phys*. **1994**, *184*, 115.
(31) Sobolewski, A. L.; Domcke, W. *Chem. Phys*. **1998**, *232*, 257.
(32) Firth, D. W.; Barbara, P. F.; Trommsdorf, H. P. *Chem. Phys*. **1989**, *136*, 349.
(33) Bisht, P. B.; Petek, H.; Yoshihara, K.; Nagashima, U. *J. Chem. Phys*. **1995**, *103*, 5290.
(34) Douhal, A.; Lahmani, F.; Zehnacker-Rentien, A. *Chem. Phys*. **1993**, *178*, 493.
(35) Domcke, W.; Stock, G. *Adv. Chem. Phys*. **1997**, *100*, 1.
(36) Roubin, P.; Chiavassa, T.; Verlaque, P.; Pizzala, L.; Bodot, H. *Chem. Phys. Lett*. **1990**, *175*, 655.
(37) Chiavassa, T.; Verlaque, P.; Pizzala, L.; Allouche, A.; Roubin, P. *J. Phys. Chem*. **1993**, *97*, 5917.
(38) Markov, P. *Chem. Soc. Rev*. **1984**, *13*, 69.
(39) Veierov, D.; Bercovici, T.; Fischer, E.; Mazur, Y.; Yogev, A. *J. Am. Chem. Soc*. **1977**, *99*, 2723.